PHYSICS AND CHEMISTRY OF SOLID STATE
V. 26, No. 1 (2025) pp. 181-189
Section: Physics

DOI: 10.15330/pcss.26.1.181-189

Vasyl Stefanyk Precarpathian National University

ФІЗИКА І ХІМІЯ ТВЕРДОГО ТІЛА
Т. 26, № 1 (2025) С. 181-189
Фізико-математичні науки

PACS: 72.15.Eb

ISSN 1729-4428 (Print)
ISSN 2309-8589 (Online)

Prashant Srivastav and Pramod Kumar Yadawa

Theoretical Investigation on Elastic, Thermal and Ultrasonic Properties of Nanostructured HfN Layers Growth on MgO (001)

Department of Physics, Prof. Rajendra Singh (Rajju Bhaiya) Institute of Physical Sciences for Study and Research, V. B. S. Purvanchal University, Jaunpur, India, pkyadawa@gmail.com

In the present study, we used higher-order elastic coefficients to compute the elastic, mechanical, and thermo-physical properties of HfN/MgO (001) nanostructured materials at temperatures ranging from 50 to 300 K. Two significant factors considered when computing the second and third-order elastic constants in the temperature range of 50 K to 300 K are the nearest-neighbor distance and the hardness parameter. We have evaluated the thermal and mechanical characteristics of the HfN/MgO (001) nanostructured layer. The analytical results of the second-order elastic constants were used to determine Young's modulus, thermal conductivity, Zener anisotropy, bulk modulus, thermal energy density, shear modulus, and Poisson's ratio. Additionally, Debye average velocity, hardness, melting temperature, and ultrasonic Grüneisen parameters (UGPs) were assessed over a range of temperatures. The fracture/toughness (B/G) ratio in this study exceeds 1.75, indicating that the HfN/MgO (001) nanostructured layer is ductile within this temperature range. The selected materials fully satisfy the Born mechanical stability criterion. It has been evaluated how long thermal relaxation takes to complete, how thermo-elastic relaxation attenuates ultrasonic waves, and how phonon-phonon interaction processes attenuate ultrasonic waves in this medium. The research results and other well-known physical characteristics are helpful for commercial applications.

Keywords: Thin layer, Elastic properties, Thermal conductivity, Ultrasonic properties.

Received 09 May 2024; Accepted 07 February 2025.

Introduction

Transition-metal nitrides are widely investigated and have become crucial in various technological applications, such as optical thin films, diffusion barriers, and hard wear-resistant coatings. The group-IVB nitrides, HfN and ZrN, which belong to the broader family of transition-metal nitrides, have garnered significant attention due to their low resistivity ($\rho < 20$ μΩ-cm), characteristic gold color from inter-band transitions, partially filled transition-metal d orbitals [1], and strong reflectivity in the red and infrared regions [2, 3]. By utilizing high-quality single crystals that have been established, the fundamental physical properties of HfN, such as electrical transport, mechanical, and optical properties, were determined as a function of alignment [3, 4]. A study of the HfN phase diagram, with nitrogen concentrations up to 50%, reported in 1990, identified the equilibrium phases as HfN with a NaCl structure, along with two stacking variations: Hf_3N_2 and Hf_4N_3, which are composed of α-Hf and HfN [5]. Additionally, there have been reports of higher nitride phases, including one with a metastable phase that is approximately Hf_3N_4 in structure [6, 7]. ZrN has also been synthesized as single crystals; however, relatively less research has been conducted on it [8, 9, 10]. Despite this, little is understood about the fundamental characteristics of HfN, an IVB nitride closely related to ZrN. HfN (001) films have been grown at 650 °C with $f N_2 = 50.07$. High-resolution X-ray diffraction (HR-XRD), high-resolution cross-sectional transmission electron microscopy (HR-XTEM), and Rutherford backscattering spectroscopy (RBS) indicate that the films are single crystalline with the B1-NaCl structure and a lattice constant (a_0) of 0.4524 nm [11-13].

The second and third-order elastic constants (SOECs and TOECs) of the HfN/MgO (001) nanostructured layer have been investigated using the Coulomb potential and Born-Mayer potential at temperatures ranging from 50 to

300 K. Using the calculated SOEC values, it is straightforward to determine the mechanical properties of this thin-layered nanostructured material, such as Poisson's ratio, fracture toughness ratio, bulk modulus, specific heat, shear modulus, Zener anisotropy factor, thermal energy density, hardness, melting temperature, and Young's modulus. Additionally, by using SOECs and TOECs, we calculated the temperature-dependent Grüneisen parameters, ultrasonic velocities, and ultrasonic attenuations along the <100>, <110>, and <111> crystallographic axes. The study also investigates how these findings relate to the physical properties of nanostructured thin films.

I. Theoretical Calculation Method

Using Born Mayer Potential approaches, the temperature-dependent higher order (second-order and third-order) non-linear elastic constant for face-centered cubic structure HfN /MgO (001) layers have been calculated.

The theoretical outline for calculating second-order elastic constants (SOECs) and third-order elastic constants (TOECs) was first developed by Brugger [14], and later refined by Ghate [15] and Mori and Hiki [16]. The estimated values of SOECs and TOECs are obtained by adding the static and vibrational contributions at a specific temperature to the elastic constants, as follows:

$$C_{ij}(T) = C_{ij}^{0} + C_{ij}^{vib} \quad \text{and} \quad C_{ijk}(T) = C_{ijk}^{0} + C_{ijk}^{vib} \qquad (1)$$

Where C_{IJ}^{0} and C_{IJK}^{0} Are strain derivatives and C_{IJ}^{Vib} and C_{IJK}^{Vib} Are strain derivatives of F^{vib}, and signify the static and vibrational elastic constants respectively. The extended expressions of elastic constants for static and vibrational terms as given as follows:

$$C_{11}^{0} = \frac{3e^2}{2r_0^4} S_5^{(2)} + \frac{1}{br_0}\left(\frac{1}{r_0} + \frac{1}{b}\right)\varphi(r_0) + \frac{2}{br_0}\left(\frac{\sqrt{2}}{2r_0} + \frac{1}{b}\right)\varphi(\sqrt{2}r_0),$$

$$C_{12}^{0} = C_{44}^{0} = \frac{3e^2}{2r_0^4} S_5^{(1,1)} + \frac{1}{br_0}\left(\frac{\sqrt{2}}{2r_0} + \frac{1}{b}\right)\varphi(\sqrt{2}r_0),$$

$$C_{111}^{0} = -\frac{15e^2}{2r_0^4} S_7^{(3)} - \frac{1}{b}\left(\frac{3}{r_0^2} + \frac{3}{br_0} + \frac{1}{b^2}\right)\varphi(r_0) - \frac{1}{2b}\left(\frac{3\sqrt{2}}{r_0^2} + \frac{6}{br_0} + \frac{2\sqrt{2}}{b^2}\right)\varphi(\sqrt{2}r_0)$$

$$C_{112}^{0} = C_{166}^{0} = -\frac{15e^2}{2r_0^4} S_7^{(2,1)} - \frac{1}{4b}\left(\frac{3\sqrt{2}}{r_0^2} + \frac{6}{br_0} + \frac{2\sqrt{2}}{b^2}\right)\varphi\left(\sqrt{2}r_0\right) \quad C_{123}^{0} = C_{144}^{0} = C_{456}^{0} = -\frac{15e^2}{2r_0^4} S_7^{(1,1,1)} \qquad (2)$$

Where e, r_o and b denote the electronic charge, nearest neighbor distance, and hardness parameter respectively. S represents the static elastic energy. Also, $\phi(r_0)$ shows the inter-ionic Born-Mayer potential approaches written by $\phi(r_0) = A \exp(-r_0/b)$ and $\phi(\sqrt{2}r_0) = A \exp(-\sqrt{2}r_0/b)$.

Here, 'A' (Strength parameter) is expressed by:

$$A = -3b\frac{e^2}{r_0^2} S_3^{(1)} \frac{1}{\left(6exp(-\rho_0) + 12\sqrt{2}\, exp\left(-\sqrt{2}r_0\right)\right)}$$

The following expressions explain the vibration term [17].

$$C_{11}^{vib} = f^{(1,1)}G_1^2 + f^{(2)}G_2$$

$$C_{12}^{vib} = f^{(1,1)}G_1^2 + f^{(2)}G_{1,1}$$

$$C_{44}^{vib} = f^{(2)}G_{1,1}$$

$$C_{111}^{vib} = f^{(1,1,1)}G_1^3 + 3f^{(2,1)}G_1G_2 + f^{(3)}G_3$$

$$C_{112}^{vib} = f^{(1,1,1)}G_1^3 + f^{(2,1)}G_1\left(2G_{1,1} + G_2\right) + f^{(3)}G_{2,1}$$

$$C_{123}^{vib} = f^{(1,1,1)}G_1^3 + 3f^{(2,1)}G_1\,G_{1,1} + f^{(3)}G_{1,1,1}$$

$$C_{144}^{vib} = f^{(2,1)}G_1\,G_{1,1} + f^{(3)}G_{1,1,1}$$

$$C_{166}^{vib} = f^{(2,1)}G_1\,G_{1,1} + f^{(3)}G_{2,1}$$

$$C_{456}^{vib} = f^{(3)}G_{1,1,1} \qquad (3)$$

The following is a list of the crystalline material born stability criteria for face-centered cubic crystals.

$$B_V = B_R = (C_{11}+2C_{12})/3 > 0;$$

$$(C_{11} - C_{12})/3 > 0; \qquad C_{44} > 0 \qquad (4)$$

The representation of the bulk modulus for elastic constants $B = (B_V + B_R)/2$, and Voigt, Hill, and Reuss average approach is indicated by the subscripts V, H, and R [18].

The theoretical estimation of shear modulus and bulk modulus has been performed using the approach described in [19]. According to Pugh, B/G defined as $G = (G_V + G_R)/2$, where $G_V = (C_{11} - C_{12} + 3C_{44})/5$ and $G_R = 5[(C_{11}-C_{12})C_{44}]/[4C_{44}+3(C_{11}-C_{12})]$. If the ratio B/G is less than 1.75, the material is brittle in nature and if this ratio is greater than 1.75, then the material is ductile [20]. Cauchy pressure P_C [21] shows the nature of bonding in a material and given by $P_C = (C_{12} - C_{44})$, the value P_C is negative for brittle materials and positive for ductile materials. Elastic anisotropy (A) projected by Zener [22] is found as $A = C_{44}/C_S$, which goes out to be the valuable condition for classifying elastically anisotropic compounds. The tetragonal shear modulus is $C_S = (C_{11} - C_{12})/2$. The expressions for Young's modulus (Y) and Poisson's ratio (σ) are stated by:

$$\sigma = (3B - 2G)/(6B + 2G), \qquad (5)$$

$$Y = 9GB/(G + 3B). \qquad (6)$$

Chen et al. [23] put forward a simple yet successful

theory for calculating Vickers hardness (Hv). This approach is effective for determining the hardness of materials.

$$H_v = 2(k^2G)^{0.585} - 3 \quad (7)$$

In addition, it is possible to predict the materials' melting point (T_m) by using elastic constant (C_{11}) and bulk modulus [24]. T_m is represented as;

$$T_m = 553 + 5.93C_{11} \pm 300, \quad (8)$$

$$T_m = 607 + 9.3B \pm 500. \quad (9)$$

Here Tm stands for the bulk modulus and also B is the melting point, respectively.

Ultrasonic velocities are an important characteristic of this transition metal layers' characterization. The orientation of the stresses will determine the specific paths along which the ultrasonic wave propagates through the anisotropic materials in directions <100>, <110>, and <111>. We obtained ultrasonic velocities, one longitudinal ultrasonic velocity (V_L) [25], and two shears ultrasonic velocities (V_{S1}, V_{S2}).

Ultrasonic attenuation leading two processes, one is the phonon-phonon interaction (Akhieser type damping) and another one is thermoelastic loss at higher temperatures. The formulations for calculation of the attenuation due to the phonon viscosity-mechanism for longitudinal and shear waves are given by Mason [26, 27]:

$$(\alpha/f^2)_{Akh.Long} = \frac{4\pi^2\tau_L E_o(D_L/3)}{2\rho V_L^3} \quad (10)$$

$$(\alpha/f^2)_{Akh.Shear} = \frac{4\pi^2\tau_S E_o(D_S/3)}{2\rho V_S^3} \quad (11)$$

Here, the acoustic coupling constants for longitudinal waves and shear waves (D_L and D_S) are provided by

$$D_L = 9 < (\gamma_i^j)^2 >_L - \frac{3<\gamma_i^j>_L^2 C_V T}{E_o}, \quad (12)$$

$$D_S = 9 < (\gamma_i^j)^2 >_S. \quad (13)$$

The following is the equation for the thermal relaxation time (τ):

$$\tau = \tau_S = \tau_L/2 = \frac{3k}{C_V V_D^2} \quad (14)$$

The Debye temperature (θ) is stated as:

$$\theta = \frac{hV_D}{k}\left[\frac{3p}{4\pi}\frac{N_A\rho}{M}\right]^{1/3} \quad (15)$$

Where p stands for atomic number. The density (ρ) and the material's molecular weight (M) are indicated.

The Debye average velocity (V_D) [28, 29] expressions are as follows:

$$V_D = \left(\frac{1}{3}\sum_{i=1}^{3}\int\frac{1}{V_i^3}\frac{d\Omega}{4\pi}\right)^{-1/3} \quad (16)$$

Thermo-elastic loss is found by:

$$(\alpha/f^2)_{Th.} = \frac{4\pi^2<\gamma_i^j>^2 kT}{2\rho V_L^5} \quad (17)$$

Here k is stand for the thermal conductivity, ω the angular frequency HfN/MgO (001) layers. γ_i^j Using the nonlinear elastic constants, one can easily evaluate the Grüneisen number.

II. Results and Discussion

The values of SOECs and TOECs are evaluated using the lattice parameter ($a=2r_0$) 4.524 and the hardness parameter (b=0.10) for HfN/MgO (001) nanostructured layer [30]. The SOECs and TOECs are evaluated using Equations (7, 8) and are presented in Table 1.

Nine elastic constants in total have been evaluated [Table 1]. Of such as four are increasing with temperature (C_{11}, C_{12}, C_{44}, C_{144}, and C_{166}) and four are decreasing with temperature (C_{111}, C_{112}, and C_{123}). It turns out that the elastic constant C_{456} is constant at all temperatures. Atomic interaction is affected by temperature, which has an impact on how stiffness constants fluctuate with it. Irrespective of whether the rigidity constants are growing or decreasing as the interatomic distance varies, As the temperature changes, the interaction potential will either rise or decrease. Other fcc-type materials have been shown to have similar types of behaviors [25, 30, 31, 32]. Elastic properties are applicable because they are connected to numerous significant solid-state phenomena, including the phonon spectra, equation of state, and interatomic potentials of HfN layers. Comparing our results with the HfN nanostructured layer C_{11} (SOEC). The evaluated value of elastic modulus is 450.90 GPa at room temperature, which is nearly similar to 450 GPa evaluated experimentally by H. S. Seo et al. [30]. As a result, HfN nanostructured layer estimates of higher-order coefficients are supported by our theoretical predictions. The selected HfN nanostructured layer is physically stable as it satisfies the Born stability criteria given in Equation 4.

From the constant resistivity, the thermal conductivity (k) is calculated using the Wiedemann-Franz law. Equations are used to determine the thermal energy density (E_0) and specific heat per unit volume (C_V) using the Debye temperatures. [29]. Table 2 presents temperature-dependent values for "k," density, thermal energy, and specific heat per unit volume.

The obtained SOECs and TOECs values are helpful for computing the bulk modulus (B), Young's modulus (Y), B/G ratio, shear modulus (G), Cauchy pressure (C_P), Poisson's ratio (σ), as well as Zener anisotropy factor (A). Temperature-dependent information presented in Figs. 1-3 demonstrates the ductility of the HfN/MgO (001) nanostructured layer at these temperatures if the ratio B/G is greater than 1.75 in the defined temperature (50-300) K. The anisotropic behavior of the HfN nanostructured layer, which is very significant in both fabrication and material physics, is demonstrated by the anisotropy coefficient that is lower than one at these temperature ranges. The Cauchy pressure (C_P) analyses the type of bonds in crystals; positive values signify substances that are more ionic as well as bonding-oriented, whereas negative values signify directional bonds [33].

Table 1.

SOECs and TOECs (GPa) of HfN layer Growth on MgO (001) substrates with temperature variations from 50K to 300K.

T [K]	C_{11}	C_{12}	C_{44}	C_{111}	C_{112}	C_{123}	C_{144}	C_{166}	C_{456}
50	478	305	349	-14.15	-64.52	-15.92	59.78	-107.3	59.77
100	489	323	349.2	-14.25	-21.67	-91.63	59.79	-107.3	59.77
150	500	350	349.4	-14.36	21.16	-167.3	59.80	-107.4	59.77
200	511	371	349.6	-14.47	64.01	-243	59.81	-107.4	59.77
250	521	402	349.8	-14.58	106.8	-318	59.82	-107.4	59.77
300	532.37	428	350	-14.68	149.7	-394.4	59.83	-107.4	59.77

Table 2.

Density (ρ), specific heat (Cv), thermal energy density (E_0), and thermal conductivity (k) of HfN layers Growing on MgO (001) substrates with temperature variations from 50K to 300K.

T [K]	k x 10^5 (erg/sec. cm. K)	ρ (gm/cm^3)	C_V x 10^6 (erg/cm^3K)	E_0 x 10^7 (erg/cm^3)
50	0.305	13.833	0.51	6.338
100	0.430	13.828	3.43	9.414
150	0.477	13.823	7.34	36.64
200	0.488	13.818	10.43	81.34
250	0.494	13.813	12.50	138.89
300	0.510	13.808	13.79	205.17

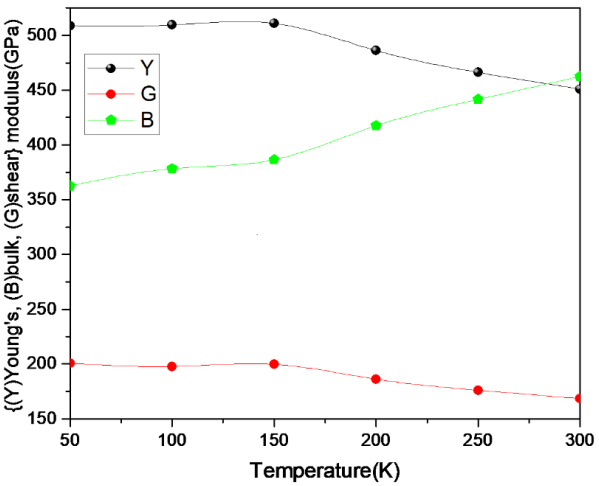

Fig. 1. Temperature-dependent Young's modulus (Y), bulk modulus (B) and shear modulus(G) of the HfN layer.

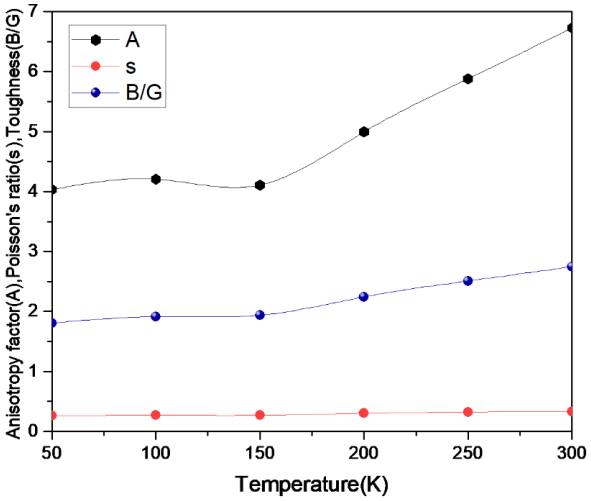

Fig. 2. Temperature-dependent anisotropy factor (A), Poisson's ratio (σ), fracture/toughness (B/G) of the HfN layer.

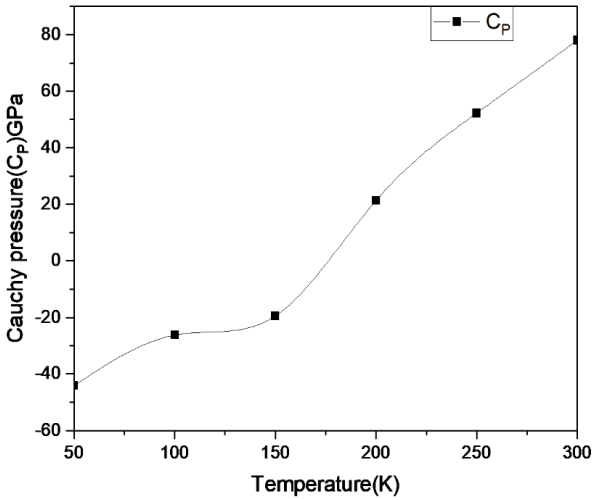

Fig. 3. Temperature-dependent Cauchy pressure (C_P)of the HfN layer.

The ultrasonic velocities of nanostructured layers are crucial metrics because they provide information on the crystallographic surface. SOECs and the density of the nano-layered materials have been used to estimate the ultrasonic velocities (V_L and V_S) for longitudinal as well as shear modes of propagation along various crystallographic axes. Also, Debye average velocity (V_D) using ultrasonic velocities is evaluated from Equation (16) and is shown in Tables 3 and 4. With rising temperatures in all directions, the ultrasonic velocities rise. Table 4 clearly shows that for the HfN thin layer, the Debye average velocity is greatest in the direction of <100>. Thus along <100> direction will be most suitable for wave propagation for this HfN thin layer deposited on MgO (001).

The thermal relaxation time (τ) is the important ultrasonic parameter, which has the time required for the re-establishment of the thermal equilibrium distribution by the strain provided by the ultrasonic wave propagation

in the crystals. A perusal of Table 4 reveals that the 'τ' decreases with temperature along all the crystallographic directions. Thermal relaxation time is found in picoseconds order for the HfN layer and is shown in Table 4. It is obvious from Eq. (14) that thermal relaxation time is relative to the thermal conductivity (k), C_V^{-1} and V_D^{-2} and a perusal of Table (2) and (4) reveals that k, Cv and V_D increase with increase the temperature.

Table 5 displays the average and squared ultrasonic Grüneisen parameter for several crystalline propagation orientations (evaluated using SOECs as well as TOECs). We used the mean parameter since these features took a range of propagation routes in different directions. Its p, which is crucial for understanding the enharmonic characteristics of nanostructured layers. Furthermore, it describes the physical characteristics of nano layer, including variations in temperature among elastic coefficients, thermal conductivity, and thermal expansion.

At various temperatures acoustical coupling constant (D) for the HfN nanoscale layer has been calculated along the different crystallographic orientations. Table 8 shows that whereas D_S is nearly constant in all three directions, we see that D_L decreases with temperature along the <100>, <110>, and <111> directions.

Table 3.

Ultrasonic velocity (10^3 m/s) of HfN layer Growth on MgO (001) substrates with temperature variations from 50K to 300K.

Direction	[100]		[110]			[111]	
T [K]	V_L	V_S	V_L	V_{S1}	V_{S2}	V_L	V_S
50	5.882	1.489	5.891	1.51	1.54	5.991	1.56
100	5.948	1.489	5.951	1.51	1.54	5.996	1.56
150	6.015	1.490	6.022	1.52	1.55	6.068	1.57
200	6.080	1.490	6.095	1.52	1.55	6.131	1.57
250	6.145	1.490	6.161	1.52	1.55	6.173	1.57
300	6.209	1.491	6.213	1.53	1.66	6.243	1.58

Table 4.

Thermal relaxation time (τ) and Debye average velocity (V_D) of HfN layers Growth on MgO (001) substrates across multiple states crystallographic orientations within the temperature range 50-300K.

T [K]	V_D (10^3 m/sec)			τ (10^{-12}sec.)		
	[100]	[110]	[111]	[100]	[110]	[111]
50	1.680	1.63	1.58	6.354	6.651	6.840
100	1.680	1.63	1.58	6.231	6.453	6.667
150	1.681	1.64	1.60	5.898	5.922	6.023
200	1.681	1.64	1.60	4.962	5.101	5.312
250	1.682	1.65	1.61	4.187	4.254	4.441
300	1.682	1.65	1.62	3.916	4.123	4.321

Table 5.

For a longitudinal wave, the average Grüneisen number $\langle\gamma_i^j\rangle_L$ for longitudinal wave, average square Grüneisen number $\langle(\gamma_i^j)^2\rangle_L$ and $\langle(\gamma_i^j)^2\rangle_S$ for longitudinal and shear wave of HfN layers Growth on MgO (001) substrates along [100] direction at temperature range 50K-300K.

T (K)	$\langle\gamma_i^j\rangle_L$	$\langle(\gamma_i^j)^2\rangle_L$	$\langle(\gamma_i^j)^2\rangle_S$
50	0.711	9.243	0.145
100	0.697	9.069	0.145
150	0.678	8.881	0.144
200	0.659	8.714	0.144
250	0.642	8.565	0.144
300	0.625	8.434	0.144

Table 6.

Average Grüneisen number $\langle\gamma_i^j\rangle_L$ for longitudinal wave, average square Grüneisen number $\langle(\gamma_i^j)^2\rangle_L$ and $\langle(\gamma_i^j)^2\rangle_S$ for longitudinal and shear wave of HfN layers Growth on MgO (001) substrates along [110] direction at temperature range 50K-300K.

T (K)	$\langle\gamma_i^j\rangle_L$	$\langle(\gamma_i^j)^2\rangle_L$	$\langle(\gamma_i^j)^2\rangle_S$
50	-1.117	11.243	0.051
100	-1.019	10.986	0.051
150	-0.979	10.663	0.051
200	-0.941	10.373	0.051
250	-0.904	10.112	0.50
300	-0.869	9.877	0.50

Table 7.

Average Grüneisen number $<\gamma_i^j>_L$ for longitudinal wave, average square Grüneisen number $<(\gamma_i^j)^2>_L$ and $<(\gamma_i^j)^2>_S$ for longitudinal and shear wave of HfN layers Growth on MgO (001) substrates along [110] direction at temperature range 50K-300K.

T (K)	$<\gamma_i^j>_L$	$<(\gamma_i^j)^2>_L$	$<(\gamma_i^j)^2>_S$
50	-1.123	6.667	11.102
100	-1.098	6.496	10.995
150	-1.068	6.205	10.998
200	-1.040	5.938	11.020
250	-1.014	5.694	11.061
300	-0.989	5.470	11.120

Table 8.

HfN layer longitudinal waves (D_L) and shear waves (D_S) Growth on MgO (001) supports a variety of crystallographic orientations between at temperature range 50K- 300 K.

T [K]	D_L			D_S			
	[100]	[110]	[111]	[100]	[100]*	[110]**	[111]
50	82.896	100.75	59.81	1.302	0.471	150.46	99.11
100	76.302	87.50	45.28	1.301	0.467	150.57	98.95
150	75.789	87.32	45.55	1.301	0.464	150.09	98.98
200	75.080	86.54	45.11	1.300	0.460	151.68	98.18
250	74.300	85.48	44.30	1.300	0.458	152.64	99.55
300	73.545	84.31	43.31	1.300	0.455	153.87	100.08

**shear wave polarized along [110], *shear wave polarized along [001]

Other face-centered cubic compounds have properties similar to those of D_S & D_L [34-36]. Because of the acoustic coupling (D_L, D_S) constants between 50 and 300 K temperature range, the attenuation remains unchanged. Thus, there is minimal effect of the nanostructured layers elastic behavior on the overall attenuation.

The hardness as well as melting temperature of the HfN/MgO (001) are determined using equations 7 and 8. Figure 4 demonstrates unequivocally how the hardness of the HfN nanostructured material diminishes as temperature increases. Figure 5 makes it abundantly evident that the melting point of the HfN layer rises as the temperature rises.

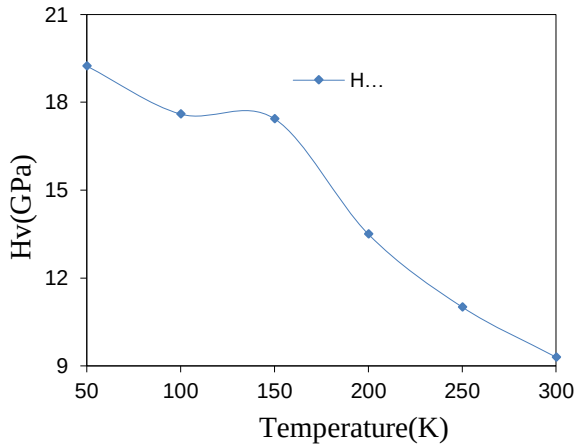

Fig. 4. Temperature-dependent hardness (H_V) of the HfN layer

Phonon-phonon interactions occur when the vibrations of atoms within a material (phonons) interact with one another. These interactions are a significant mechanism behind energy dissipation when sound waves (ultrasonic waves) propagate through the material. As phonons scatter off each other, part of the energy from the sound wave is lost, which contributes to ultrasonic attenuation.

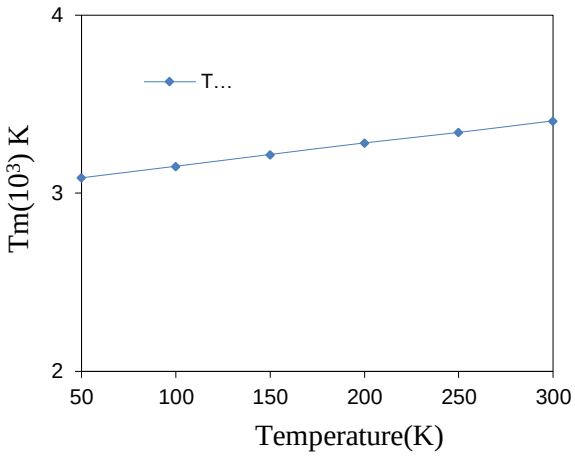

Fig. 5. Temperature-dependent melting temperature (T_m) of the HfN layer.

The attenuation of ultrasonic waves in a material is not only governed by phonon-phonon interactions but also by the crystalline structure and defects present, especially at the nanoscale. Defects such as vacancies, dislocations, and grain boundaries significantly influence the scattering of phonons, which leads to greater energy dissipation and increased ultrasonic attenuation. Therefore, a comprehensive understanding of how phonon-phonon interactions correlate with material structure and defects at the nanoscale is essential for designing materials with desired acoustic properties.

Along different crystallographic directions, the

temperature-dependent ultrasonic attenuation has been estimated for the HfN layer using Equations 10, 11 and 17 under the condition $\omega\tau<<1$ and is shown in Figures 6-8. The Akhieser loss of energy for longitudinal waves, shear waves and also thermoelastic loss increases with the temperature. Figures 6-8 also designate that the ultrasonic attenuation due to thermoelastic relaxation and shear wave are smaller in comparison to the attenuation due to longitudinal wave. Thus, thermal conductivity as well as thermal energy density are the primary driving forces behind this behavior. Understanding the contribution of microstructural events, related physical characteristics, and associated scientific factors to total ultrasonic attenuation at high temperatures is crucial.

Low temperatures exhibit the relatively low thermal loss attenuation $(\alpha/f^2)_{Th}$, whereas room temperature exhibits the maximum attenuation (300K). Thermal conductivity & thermal loss are inversely connected, with minima and peaks occurring as temperature increases. Phonon-phonon interaction occurs in the HfN nanostructured layer because thermal losses have a smaller effect on ultrasonic attenuation than some other types of losses.

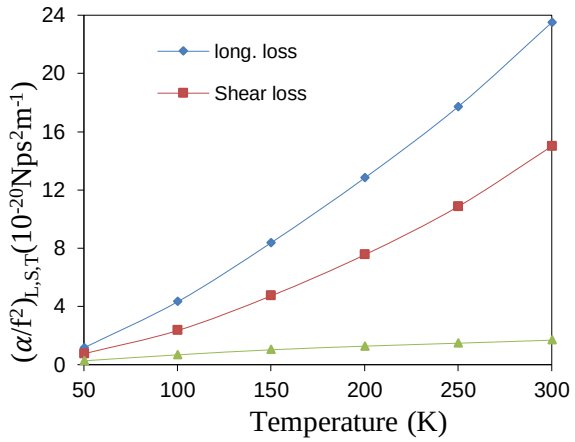

Fig. 6. Ultrasonic Attenuation $(\alpha/f^2)_{Th}$, $(\alpha/f^2)_{Akh.\ Long}$ and $(\alpha/f^2)_{Akh.\ Shear}$ along [100] direction in the HfN nanostructured layer

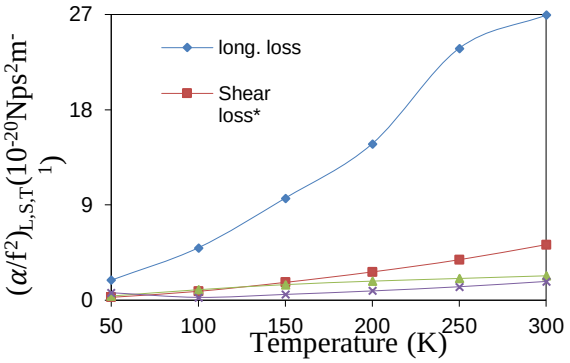

Fig. 7. Ultrasonic Attenuation $(\alpha/f^2)_{Th}$, $(\alpha/f^2)_{Akh.\ Long}$ and $(\alpha/f^2)_{Akh.\ Shear}$ along [110] direction in the HfN layer. *Shear wave polarized along [001] and **shear wave polarized along [1$\bar{1}$0].

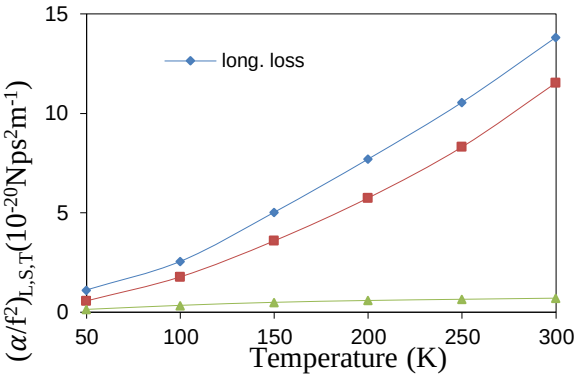

Fig. 8. Ultrasonic Attenuation $(\alpha/f^2)_{Th}$, $(\alpha/f^2)_{Akh.\ Long}$ and $(\alpha/f^2)_{Akh.\ Shear}$ along [111] direction in the HfN layer.

Conclusions

Based on the above discussion is worthwhile to state that:

At various temperature ranges 50K-300K, the higher-order elastic coefficients of the HfN nanostructured layer are evaluated using the Coulomb and Born-Mayer potentials approaches.

Relevant elastic characteristics, such as bulk modulus, Poisson's ratio, shear modulus, and Young's modulus are also evaluated at this temperature range.

For the objective of calculating strength, the fracture to toughness ratio, Zener anisotropy coefficient, and Cauchy pressures of this nanostructured layer have been evaluated, it is possible to further estimate the mechanical properties of HfN, such as ductile-brittle characteristics and elastic anisotropy.

The study demonstrates that the HfN layer is mechanically strong, ductile, and displays anisotropy on flexibility within the range of temperature of 50-300 K.

Elastic constants can be used to compute the hardness of the HfN nanostructured layer, and within this specific temperature range, the hardness decreases with increasing temperature. Considering the HfN nanostructured layer shortest thermal relaxation time, the thermal phonon distribution has to return to equilibrium in a very short amount of period—roughly picoseconds. Along the <100>, <110>, and <111> crystallographic orientations, ultrasonic velocities and average Grüneisen numbers are determined.

This work utilizes multiple crystallographic axes to figure out the acoustic coupling coefficients for both longitudinal and shear waves. The ultrasonic attenuation rises with temperature in all crystallographic orientations; however, it is least at lower temperatures (50 K) than at room temperature (300 K).

This study could be useful for processing as well as non-destructive evaluation of the HfN nanostructured layer growing on MgO (001). These findings will operate as the starting point for investigation into the essential thermal as well as mechanical properties of additional nanoscale materials. The small dimensions of nanostructured layers can lead to stronger light scattering and absorption, which can be beneficial for coatings that need to manage light interaction, such as solar cells or optical sensors.

Acknowledgments
Authors are thankful to Center of Excellence grant from Department of Higher Education, Uttar Pradesh for financial support.

Srivastav Prashant – Ph. D. Research Scholar;
Yadawa Pramod Kumar – Professor.

[1] C. Stampfl, W. Mannstadt, R. Asahi, A. J. Freeman, *Electronic structure and physical properties of early transition metal mononitrides: Density-functional theory LDA, GGA, and screened-exchange LDA FLAPW calculations* Phys. Rev. B, 63, 155106 (2001); https://doi.org/10.1103/PhysRevB.63.155106.
[2] A. Delin, A.O. Eriksson, R. Ahuja, B. Johansson, M.S.S. Brooks, T. Gasche, S. Auluck, J.M. Wills, *Optical properties of the group-IVB refractory metal compounds. Phys. Rev. B*, 54, 1673 (1996); https://doi.org/10.1103/PhysRevB.54.1673.
[3] J. E. Sundgren, B. O. Johansson, A. Rockett, S. A. Barnett, J.E. Greene, *Physics and Chemistry of protective coatings*, AIP Conf. Proc. No. 149 AIP, New York, 95 (1986).
[4] C. S. Shin, D. Gall, N. Hellgren, J. Patscheider, I. Petrov, J. E. Greene, *Vacancy hardening in single-crystal TiNx (001) layers*, J. Appl. Phys. 93, 6025 (2003); https://doi.org/10.1063/1.1568521.
[5] T.B. Massalski, ASM International Metals Park 2090, (1990).
[6] B.O. Johansson, U. Helmersson, M.K. Hibbs, J.E Sundgren, *Reactively magnetron sputtered HfN films II. Hardness and electrical resistivity*, J. Appl. Phys.k 58, 3104 (1985); https://doi.org/10.1063/1.335813.
[7] N. Savvides, B. Window, *Electrical transport, optical properties, and structure of TiN films synthesized by low energy ion-assisted deposition*, J. Mater. Res.k 1, 224 (1986); https://doi.org/10.1063/1.341468.
[8] S.A. Barnett, L. Hultman, J.E. Sundgren, F. Ronin, S. Rohde, *Epitaxial growth of ZrN on Si (001)*, Appl. Phys. Lett., 53, 400 (1988); https://doi.org/10.1063/1.99891.
[9] K. Tanabe, H. Asano, Y. Katoh, O. Michigami, *Properties of Superconducting ZrN Thin Films Deposited by dc Reactive Magnetron Sputtering*, Japanese J. Appl. Phys., 26, 570 (1970).
[10] H. Yanagisawa, K. Sakaki, Y. Abe, M. Kawamura, S. Shinkai, *Epitaxial Growth of (001) ZrN Thin Films on (001) Si by Low Temperature Process*, Japan J. Appl. Phys., 44, 343 (2005);
[11] R. D. Bringans, P. Steiner, T. Wolf, *Photoemission study of the electronic structure of stoichiometric and sub stoichiometric TiN and ZrN*, Phys. Rev. B, 25, 7183(1982).
[12] H. Ljungcrantz, M. Oden, L, Hultman, J. E. Greene, J. E. Sundegren, *Nano indentation studies of single-crystal (001) -, (011) -, and (111) -oriented TiNx layers on MgO*, J. Appl. Phys., 80, 6725(1995); https://doi.org/10.1063/1.363799.
[13] P. Villars, L. D. Calvert, *Person's handbook of crystallographic data for intermetallic phases*, ASM International, Materials Park OH (1991).
[14] K. Brugger, *Thermodynamic Definition of Higher Elastic Coefficients*, Phys. Rev., 133, A1611 (1964); https://doi/10.1103/PhysRev.133.A1611.
[15] P.B. Ghate, *Third-Order Elastic Constant of Alkali Halide Crystals*, Phys. Rev., 139, A1666 (1965); https://doi.org/10.1103/PhysRev.139.A1666.
[16] S. Mori, Y. Hiki, *Calculations of the Third and Fourth-Order Elastic Constants of Alkali Halide Crystals*, J. Phys. Soc. Japan, 45, 1449 (1975): https://doi/10.1143/JPSJ.45.1449.
[17] P. K. Yadawa, R. R. Yadav, *Ultrasonic Study of Intermediate-valent Intermetallic $YbAl_2$ at different physical conditions*, Multidiscipline Modelling in Materials and Structures, 5, 59 (2009); https://doi.org/10.1108/15736105200900004.
[18] R. Hill, *The Elastic Behavior of Crystalline Aggregate*, Proc. Phys. Soc. Sec. A, 65, 349 (1952); https://doi.org/10.1088/0370-1298/65/5/307.
[19] D. Singh, S. Kaushik, S. Tripathi, V. Bhalla, A. K. Gupta, *Mechanical and thermo-physical properties of the rare earth Monopnictides*, Arab J Sci Eng., 39, 485 (2014); https://doi.org/10.1007/s13369-013-0845-1.
[20] S. F. Pugh, *Relation between the elastic moduli and the plastic properties of polycrystalline pure metals*, Philos. Mag., 45, 823 (1954); https://doi.org/10.1080/14786440808520496.
[21] D. G. Pettifor, *Theoretical predictions of structure and related properties of intermetallic*, Mater. Sci. Technol., 8, 345 (1992); https://doi.org/10.1179/mst.1992.8.4.345.
[22] S. Bhajanker, V. Srivastava, G. Pagare, S.P. Sanyal, J. Phys. Conf. Ser., 377 (2012); https://link.springer.com/article/10.1007/s10765-016-2038-0.
[23] Q.X. Chen, H. Niu, D. Li, Y. Li, *Modeling Hardness of Polycrystalline Materials and Bulk Metallic Glasses*, Intermetallics, 199, 1275 (2012); https://link.springer.com/article/10.1007/s10765-016-2038-0.
[24] M.E. Fine, L.D. Brown, H.L. Marcus, *Elastic Constants versus Melting Temperature in Metals*, Scripta Metall., 18, 951 (1984); https://doi.org/10.1016/0036-9748(84)90267-9.
[25] V. Bhalla, D. Singh, S. K. Jain, *Mechanical and thermo-physical properties of the rare earth Monopnictides*, International Journal of Computational Materials Science and Engineering, 5, 1650012 (2016); http://dx.doi.org/10.1142/S2047684116500123.
[26] W. P. Mason, Academic Press Inc., 237, (1965); https://www.worldcat.org/title/physical-acoustics-principles-and-methods-vol-1-part-a/oclc/463203402.

[27] W.P. Mason, *Relation between Third order Elastic Moduli and the Thermal Attenuation of Ultrasonic Wave in Non-conducting and Metallic Crystals*, J. Acoustic Soc., 40**,** 852 (1966); https://doi.org/10.1121/1.1910158.
[28] D.E. Gray, AIP Handbook, 3rd edition (New York, Mc Graw Hill Co. 1956); http://web.ipb.ac.id/~erizal/hidrolika/Chow%20-%20OPEN%20CHANNEL%20HYDRAULICS.pdf.
[29] C. Oligschleger, R.O. Jones, S. M. Riemann, H. R. Schober, *Erratum: Model interatomic potential for simulations in selenium*, Phys. Rev., 102**,** 6165 (2020); https://doi.org/10.1103/PhysRevB.102.099901.
[30] H.S. Seo, T.Y. Lee, I. Petrov, J.E. Greene, *Growth and physical properties of epitaxial HfN layers on MgO (001)*, J. Appl. Phys., 96**,** 878 (2004); https://doi.org/10.1063/1.1759783.
[31] M. Landa, V. Novak, P. Sedlak, P. Sittner, *Ultrasonic characterization of Cu, Al, Ni single crystals lattice stability in the vicinity of the phase transition*, Ultrasonics, 42, 519 (2004); https://doi.org/10.1016/j.ultras.2004.01.029.
[32] A.K. Prajapati, S. Rai, P. Srivastav, P. K. Yadawa, *Theoretical investigation on mechanical, thermal and ultrasonic properties of epitaxial nanostructured ZrN layers growth on MgO (001) substrate*, Chem.Phys. Mater., 2, 253 (2023); https://doi.org/10.1016/j.chphma.2023.02.003.
[33] V. Kanchana, G. Vaitheeswaran, X. Zhang, Y. Ma, A. Svane, O. Eriksson, *Lattice dynamics and elastic properties of 4f electron system: CeN*, Phys. Rev. B, 84, 205135 (2011); http://dx.doi.org/10.1103/PhysRevB.84.205135.
[34] N. Yadav, S.P. Singh, A.K. Maddheshiya, P.K. Yadawa, R.R. Yadav, *Mechanical and thermo-physical properties of high-temperature* Ir_xRe_{1-x} *alloys*, Phase Transitions, 93, 883 (2020); https://doi.org/10.1080/01411594.2020.1813290.
[35] P.K. Yadawa, *Effect of temperature dependent ultrasonic velocities and attenuation of GaP nanowire*, Journal of theoretical and applied physics, 10, 1 (2016); https//doi.org/10.1007/s40094-016-0216-x.
[36] D. Singh, P.K. Yadawa, S.K. Sahu, *Effect of electrical resistivity on ultrasonic attenuation in NpTe*, Cryogenics, 50, 476 (2010); https://doi.org/10.1016/j.cryogenics.2010.04.005.

Прашант Шрівастав і Прамод Кумар Ядава

Теоретичні дослідження пружних, теплових та ультразвукових властивостей наноструктурованих шарів HfN на MgO (001)

Кафедра фізики, Інститут фізичних наук для вивчення та досліджень ім. професора Раджендра Сінгх (Раджу Бхайя), університет V. B. S. Purvanchal, Джаунпур, Індія, pkyadawa@gmail.com

У цьому дослідженні для обчислення пружних, механічних і теплофізичних властивостей наноструктурованих матеріалів HfN/MgO (001) в діапазоні температур від 50 до 300 К використано коефіцієнти пружності вищого порядку. Два важливі фактори, які враховуються при обчисленні постійних пружності другого та третього порядку в діапазоні температур від 50 К до 300 К, це відстань найближчого сусіда та параметр твердості. Оцінено термічні та механічні характеристики наноструктурного шару HfN/MgO (001). Аналітичні результати пружних констант другого порядку використано для визначення модуля Юнга, теплопровідності, анізотропії Зенера, об'ємного модуля, густини теплової енергії, модуля зсуву та коефіцієнта Пуассона. Крім того, середня швидкість за Дебаєм, твердість, температура плавлення та ультразвукові параметри Грюнайзена (UGP) були оцінені залежно від температури. Співвідношення руйнування / в'язкість (B/G) у цьому дослідженні перевищує 1,75, що вказує на те, що наноструктурований шар HfN/MgO (001) є пластичним у цьому діапазоні температур. Вибрані матеріали повністю задовольняють критерію механічної стійкості Борна. Було оцінено, скільки часу займає термічна релаксація, як термопружна релаксація послаблює ультразвукові хвилі та як процеси фонон-фононної взаємодії послаблюють ультразвукові хвилі в цьому середовищі. Результати досліджень та інші добре відомі фізичні характеристики корисні для комерційного застосування.

Ключові слова: Тонкий шар, Пружні властивості, Теплопровідність, Ультразвукові властивості.